Microsc. Microanal. 19, S5, 119–122, 2013
doi:10.1017/S1431927613012464

IUMAS

Microstructure Characterization of Defects in Cubic Silicon Carbide Using Transmission Electron Microscopy

Bralee Chayasombat,[1] Yusuke Kimata,[1] Tomoharu Tokunaga,[2] Kotaro Kuroda,[2] and Katsuhiro Sasaki[2,*]

[1] *Graduate School of Engineering, Nagoya University, Furo-cho Nagoya 464-8603, Japan*
[2] *Department of Quantum Engineering, Nagoya University, Furo-cho Nagoya 464-8603, Japan*

Abstract: Microstructures of 3C–SiC grown by chemical vapor deposition (CVD) technique on undulant silicon substrate and a further developed technique called switch-back epitaxy (SBE) were studied using transmission electron microscopy (TEM). In case of the CVD sample, the density of the stacking faults was found to be significantly decreasing along growth direction. Sites of collision of stacking faults were observed using high-resolution transmission electron microscopy. Some of the stacking faults were observed to have disappeared after colliding into each other. The stacking faults were identified to be on the same type of plane and had the same type of displacement vector not only in CVD and SBE but also in the epitaxial layer on the SBE SiC samples.

Key words: CVD 3C–SiC, SBE 3C–SiC, epitaxial layer, stacking fault, FIB, TEM

Introduction

Silicon carbide (SiC) has many attractive properties such as wide band gap, high breakdown electrical field, and high thermal conductivity that make it attractive as a high-power, high-frequency, and high-temperature semiconductor material for replacing silicon-based semiconductors. Among various polytypic structures of SiC, 3C–SiC possesses a unique cubic structure and has the highest electron mobility [1,000 cm^2/Vs for 3C–SiC and 600 cm^2/Vs for 6H–SiC (Harris, 1995)] and also a lower density of interface states between SiC and SiO_2 than hexagonal SiC (Ciobanu et al., 2003). Because of its lowest band gap among SiC polytypes, 3C–SiC is believed to have the lowest interface-state traps. These properties make 3C–SiC attractive as a more suitable material for metal-oxide semiconductor field-effect transistors. However, during the crystal growth of 3C–SiC, defects such as stacking faults are easily induced in 3C–SiC. These defects strongly restrict the development of 3C–SiC as a device material. The fabrication of low defect density substrate is the main issue in the research of 3C–SiC.

In this study, microstructures of 3C–SiC were characterized using transmission electron microscopy (TEM) and high-resolution transmission electron microscopy (HRTEM). The objective in this study is to compare and characterize the defects in 3C–SiC fabricated by the chemical vapor deposition (CVD) method and a further developed method for reducing the density of defects.

Experimental Procedures

Two types of 3C–SiC wafers were provided by HOYA, the CVD 3C–SiC and the switch-back epitaxy (SBE) 3C–SiC, and developed by HOYA in 2006. Details for the growth method for CVD 3C–SiC can be found in the reference Nagasawa and Yamaguchi (1993), Nagasawa et al. (2002), and for SBE 3C–SiC in Yagi et al. (2006). The TEM specimens were thinned by the focused ion beam (FIB) technique, and examined in a JEOL 200CX and JEM 2010 at an accelerating voltage of 200 kV.

Results and Discussion

Defects in CVD 3C–SiC

Figure 1a shows a cross-sectional TEM image of CVD 3C–SiC near the Si/SiC interface. The observation was made along the $[1\bar{1}0]$ direction. Three kinds of stacking faults can be observed as indicated in the lines 1, 2, and 3. In order to evaluate the relative change of stacking density, the number of stacking faults crossing the line that is running parallel to the Si/SiC interface was counted. Figure 1b shows counts of stacking fault 1 and 2 per length along the line parallel to the Si/SiC interface, which can be referred to as (111) and $(\bar{1}\bar{1}1)$ stacking fault density, versus distance from the Si/SiC interface. It can be seen that both types of stacking fault are decreasing along the growth direction. The stacking fault 3 can be referred to as the stacking fault in $(\bar{1}1\bar{1})$ or $(1\bar{1}\bar{1})$, and was found not to decrease along the growth direction (Nagasawa & Yamaguchi, 1993; Nagasawa et al., 2002).

Figures 2a–2f show HRTEM images of collision sites of (111) and $(\bar{1}\bar{1}1)$ stacking faults taken with $1\bar{1}0$ zone axis. From these images, the collision can be categorized into four kinds. Figure 2a shows the commonly observed site collision where both the stacking faults disappeared. Figure 2b shows the collision site where the crystal structure of 3C–SiC had collapsed and formed complicated multiple stacking faults structure. Figures 2c and 2d show the collision site where one of the stacking faults disappeared and

© MICROSCOPY SOCIETY OF AMERICA 2013
*Corresponding author. E-mail: khsasaki@nagoya-u.jp

https://doi.org/10.1017/S1431927613012464 Published online by Cambridge University Press

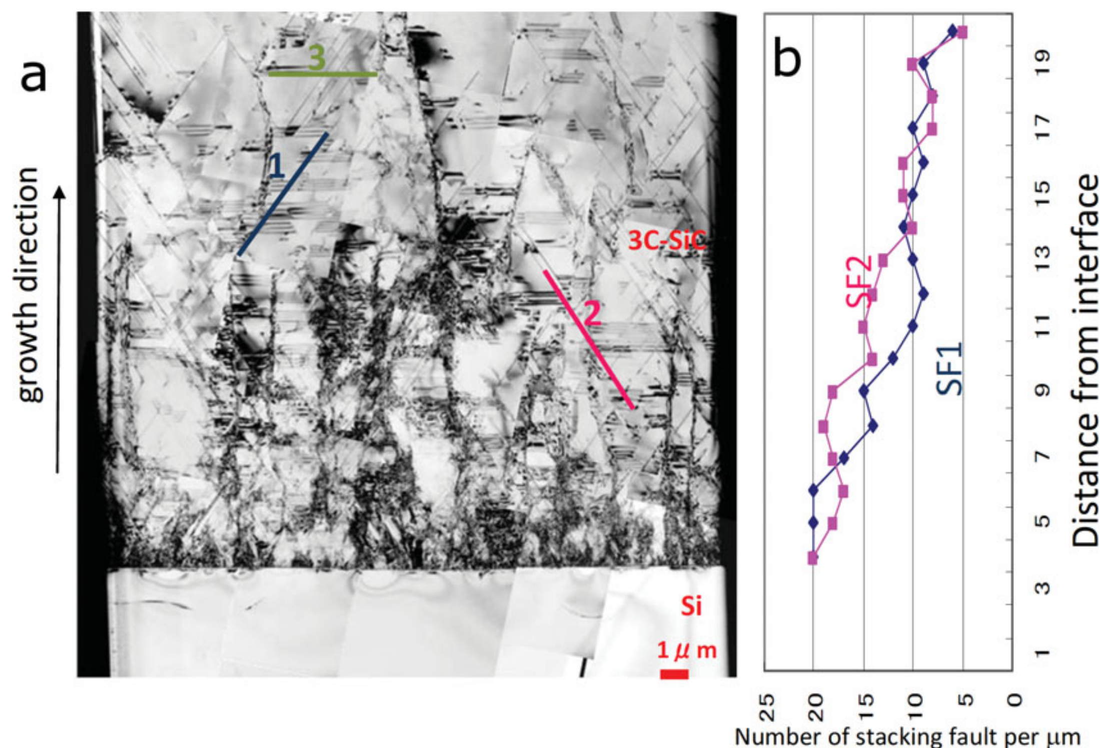

Figure 1. **a**: Cross-sectional transmission electron microscopy image of chemical vapor deposition-SiC near the Si/SiC interface. **b**: Number of stacking fault versus distance from the interface.

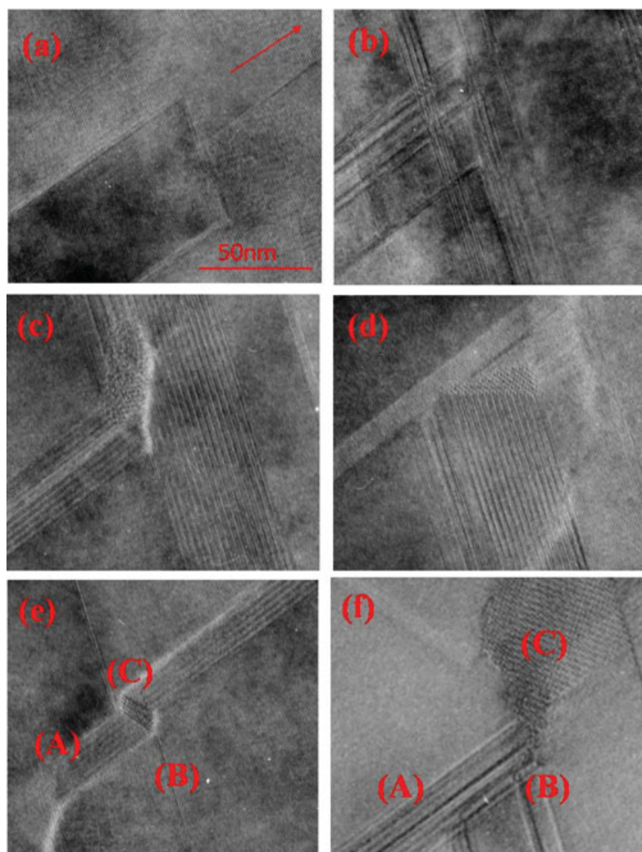

Figure 2. **a–f**: High-resolution transmission electron microscopy images of collision sites of stacking faults.

the other survived. Figures 2e and 2f show that after collision of stacking fault (A) and (B), a new type of stacking fault (C), perhaps in $(\bar{1}1\bar{1})$ or $(1\bar{1}\bar{1})$, appeared. It has been reported (Kaiser et al., 2001) that the stacking faults in {111} planes in 3C–SiC follow the Shockley partials with the (1/6)⟨112⟩-type Burgers vectors ***b***. The intersection of (111) and $(\bar{1}\bar{1}1)$ causes the interaction between two partials with the ***b*** of (1/6)⟨112⟩ lying on (111) or $(\bar{1}\bar{1}1)$. As the results, three of nine cases lead the formation of (1/6)⟨110⟩ sessile dislocations or two of nine cases lead the formation of (1/3)⟨001⟩ sessile dislocations, which could terminate both the stacking faults as shown in Figure 2a. However, in other cases, the above-mentioned sessile dislocations cannot be formed, which correspond to Figures 2b–2f.

The reduction of (111) and $(\bar{1}\bar{1}1)$ stacking fault was believed to occur because of the growth on the undulant silicon substrate (Nagasawa & Yamaguchi, 1993; Nagasawa et al., 2002). The (001) silicon substrate was undulated in the $[1\bar{1}0]$ direction. Therefore, the SiC is believed not to grow along the [100] direction, but rather along the [111] or $[\bar{1}\bar{1}1]$ direction at the initial stage of the growth. Owing to the difference in the lattice parameter of silicon and SiC, four types of {111} stacking faults would be formed. As the growth continues, (111) and $(\bar{1}\bar{1}1)$ stacking fault would easily be formed; however, they collide into each other and disappear. The above-mentioned HRTEM results suggest that the collision of (111) and $(\bar{1}\bar{1}1)$ stacking faults gives the incomplete disappearance of the faults in some case, which could limit the reduction of the defect in the CVD 3C–SiC. On the contrary, the $(1\bar{1}\bar{1})$ and $(\bar{1}1\bar{1})$ stacking faults are not

https://doi.org/10.1017/S1431927613012464 Published online by Cambridge University Press

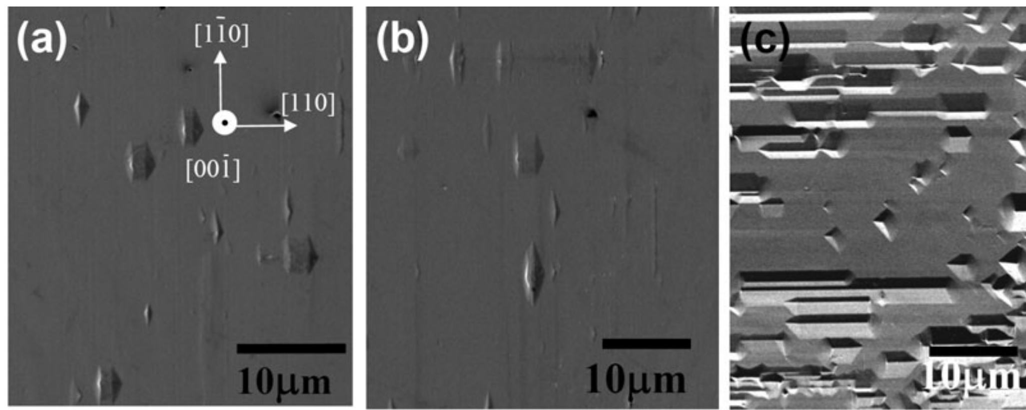

Figure 3. SIM image of the surface of switch-back epitaxy (**a**) as-grown, (**b**) with 14 μm, and (**c**) with 28 μm of epitaxial layer after etching.

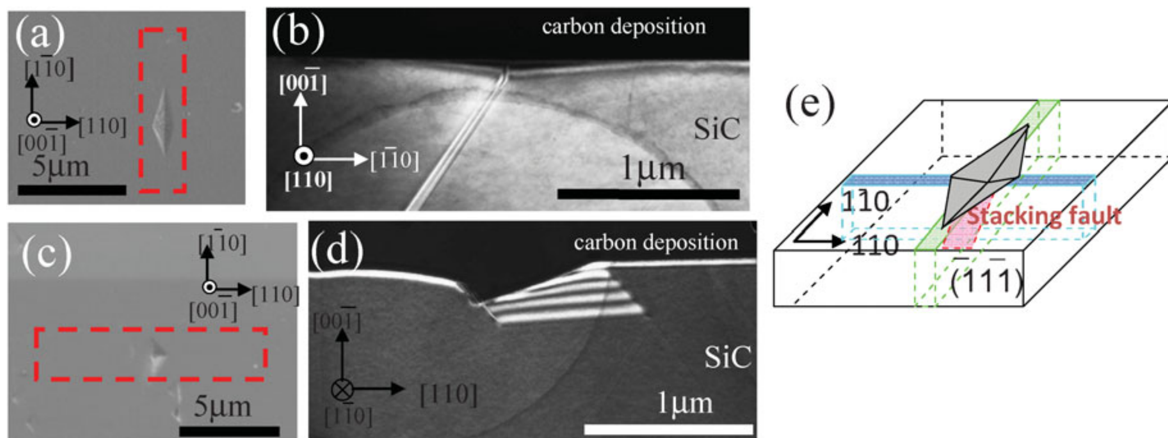

Figure 4. a: SIM image of the surface of 3C–SiC after etching and (**b**) (1$\bar{1}$0) cross-sectional transmission electron microscopy image corresponding to the region indicated by the broken-line square in (**a**). In a similar manner, (**c**) SIM image and (**d**) corresponding (110) cross-section indicated in (**c**). **e**: Schematic drawing showing the geometry of the stacking fault and the etch pit.

parallel to the growth direction, and thus they would hardly be formed, and do not disappear by collision into each other.

Defects in SBE 3C–SiC

Owing to the low defect density, the surface of the crystal was etched by HF–HNO_3 solution to identify the defects position and allow the site-selective cross-sectional TEM specimen preparation. In the other point of view, as for the device application, the defects exposing to the surface is important. The epitaxial layer grown on the postgrown crystal is also important for the device fabrication. The characterization of the defects on the surface of the as-grown SBE crystal and the epitaxial layer on the SBE crystal was performed. For comparison of the time evolution of the defects in the epitaxial layer, as grown and two types of SBE 3C–SiC with 14 and 28 μm of epitaxial layer were etched as shown in Figures 3a, 3b, and 3c, respectively. Rhombic etch pits are observed on the surfaces of the as-grown crystal and the 14 μm of epitaxial layer. The density of the etch pit was $\sim 1.2 \times 10^4/\text{cm}^2$ on both surfaces. As the epitaxial layer thickens, the etch pits were expanded along the [110] direction, as observed in longer defect lines in Figure 3d. The measured defect density on the surface of the 28 μm epitaxial layer was $\sim 1.7 \times 10^4/\text{cm}^2$. Although there was an abrupt change in the morphology of the etch pits, the density of defects showed only a gradual increase.

In order to identify the defects at which the etch pit was formed, the cross-sectional TEM observations were performed. Figures 4a and 4c show the SIM image of the surface of SBE 3C–SiC after etching, and Figures 4b and 4d show the (1$\bar{1}$0) and (110) cross-sectional dark-field TEM image observed along the [110] and [1$\bar{1}$0] direction, respectively, which were perpendicular to each other. The relationship between the figure of the etch pit and the alignment of the stacking fault indicate can be shown in Figure 4e. The stacking faults observed in the SBE crystal were on ($\bar{1}$1$\bar{1}$), which is one of the residual stacking fault types in SBE crystal. The defect identification on the surface of 14 and 28 μm of epitaxial layers also showed completely identical result of as grown crystal. The expansion of the etch pit along [110] on 28 μm of epitaxial layers could be under-

https://doi.org/10.1017/S1431927613012464 Published online by Cambridge University Press

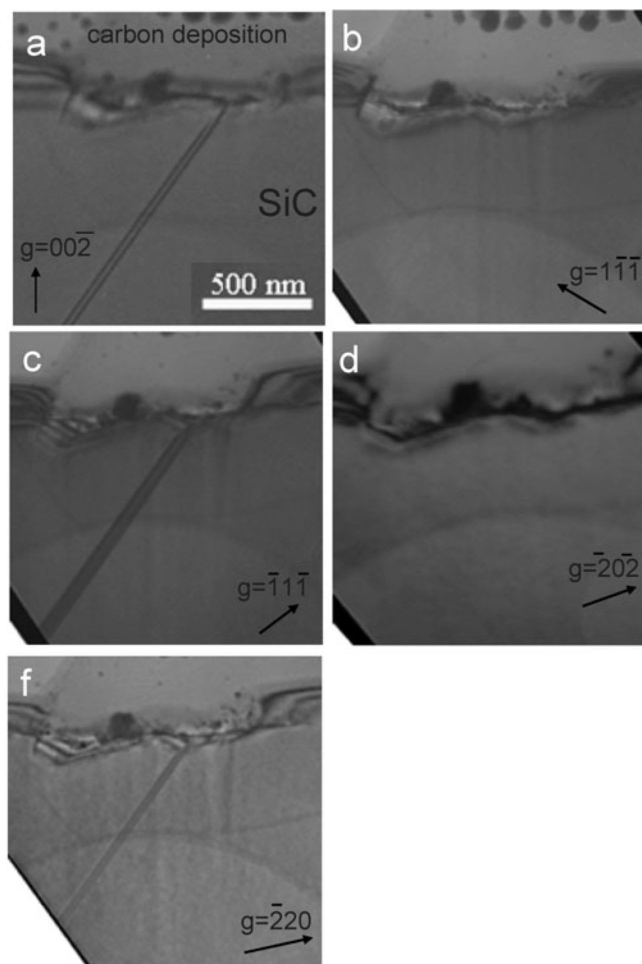

Figure 5. **a–e**: Dark-field images of 3C–SiC taken under the **g** = $00\bar{2}$, $1\bar{1}\bar{1}$, $\bar{1}1\bar{1}$, $\bar{2}0\bar{2}$, and $\bar{2}20$, respectively.

stand as the lateral growth of stacking fault which crossed the surface along [110]. It could be deduced that one of the two types of stacking faults included in the SBE crystal, i.e., $(1\bar{1}\bar{1})$ and $(\bar{1}1\bar{1})$, is thought to be observed on the surface. Also, the deduction suggests that the defects in the epitaxial layer were originating from the defects which were on the surface of the SBE crystal.

A contrast experiment was conducted in order to characterize the displacement vector **R** of the stacking fault in the epitaxial layer. Figure 5 shows bright field images of a cross-section of an etch pit in Figure 3b along the longer axis. As shown, a stacking fault existed at the bottom of the etch pit. Figures 5a–5e show bright field images in a two-beam condition using the **g** = $00\bar{2}$, $1\bar{1}\bar{1}$, $\bar{1}1\bar{1}$, $\bar{2}0\bar{2}$, and $\bar{2}20$, respectively. The contrast of the stacking fault is invisible, i.e., $\mathbf{g} \cdot \mathbf{R} = 0$, under the $\mathbf{g} = 1\bar{1}\bar{1}$ and $\mathbf{g} = \bar{2}0\bar{2}$ conditions. Accordingly, the displacement vector of the observed stacking fault was identified to be $\mathbf{R} = 1/6[\bar{1}\bar{2}1]$, and **R** lay in the $(\bar{1}1\bar{1})$ plane. This result agrees well with the result of the study on CVD and SBE 3C–SiC. The stacking faults in CVD, SBE, and the epitaxial layer on SBE 3C–SiC can be concluded to be the same type. The common nature of the defects in the SBE crystal and the epitaxial layer also suggests that the defects in the epitaxial layer are originating in the defects of base crystals.

Summary

Microstructures of CVD 3C–SiC were investigated by TEM. Decrease of defects along the growth direction was observed. A comparison between the CVD 3C–SiC and the SBE 3C–SiC was made. It was found that although the SBE SiC have a lower concentration of the defects, the type of the defect is the same as the CVD SiC, which are stacking faults aligned along the {111}. The displacement vector and the fault plane of the stacking faults in the epitaxial layer on SBE 3C–SiC was identified as $\mathbf{R} = 1/6[\bar{1}\bar{2}1]$ and on $(\bar{1}1\bar{1})$ by contrast experiment, respectively. It can be concluded that the stacking faults are of the same type in CVD and SBE, as well as in the epitaxial layer on SBE 3C–SiC.

Acknowledgment

The materials were supplied by Dr. Nagasawa of HYOA company. The authors gratefully acknowledge this support.

References

Ciobanu, F., Pensl, G., Nagasawa, H., Schoner, A., Dimitrijev, S., Cheong, K.-Y., Afanas'ev, V.V. & Wagner, G. (2003). Traps at the interface of 3C-SiC/SiO_2-MOS-structures. *Mater Sci Forum* **433–436**, 551–554.

Harris, G.L. (1995). *Properties of Silicon Carbide*. London: Institution of Electrical Engineers.

Kaiser, U., Khodos, I., Kovalchuk, M. & Richter, W. (2001). Partial dislocations and stacking faults in cubic SiC. *Crystallogr Rep* **46**, 1005–1013.

Nagasawa, H., Yagi, K. & Kawahara, T. (2002). 3C-SiC heteroepitaxial growth on undulant Si(0 0 1) substrate. *J Cryst Growth* **237–239**, 1244–1249.

Nagasawa, H. & Yamaguchi, Y. (1993). Atomic level epitaxy of 3C-SiC by low pressure vapour deposition with alternating gas supply. *Thin Solid Films* **225**, 230–234.

Yagi, K., Kawahara, T., Hatta, N. & Nagasawa, H. (2006). 'Switch-Back Epitaxy' as a novel technique for reducing stacking faults in 3C-SiC. *Mater Sci Forum* **527–539**, 291–294.

https://doi.org/10.1017/S1431927613012464 Published online by Cambridge University Press